tion constant $K_a = 201\ l\ mol^{-1}$, $\Delta G = 3.1$ kcal mol^{-1} for 1,4-dimethoxybenzene; $K_a = 200\ l\ mol^{-1}$, $\Delta G = 3.1$ kcal mol^{-1} for 1,4-dicyanobenzene in D_2O at 25 °C. Double-differential complexation can produce approximately double the magnitude of ΔG, making the structure of **1** stable enough to assemble quantitatively at high concentration.

Such an interpretation is consistent with remarkable medium effect that enabled the equilibrium ratio **1**:**2** to be varied over the range of >99:<1 to <1:>99 (Table 1). Thus the use of a more polar median (D_2O solution of $NaNO_3$) increased the ratio of **1** up to >99% even at a low concentration, owing probably to enhanced hydrophobic interaction in the catenane formation (runs 1–4). In contrast, the ratio of **1** diminished with a less polar medium (CD_3OD–D_2O, runs 9–11). Selective stabilization of **2** by adding sodium (*p*-methoxyphenyl)acetate (**9**), a specific guest for **2**, also reduced the ratio **1**:**2** (runs 6–8). □

Received 13 December 1993; accepted 11 January 1994.

1. Wasserman, E. *J. Am. chem. Soc.* **82,** 4433–4434 (1960).
2. Dietrich-Buchecker, C. O. & Sauvage, J.-P. *Chem. Rev.* **87,** 795–810 (1987).
3. Ashton, P. R. *et al. Angew. Chem. int. Edn engl.* **28,** 1396–1399 (1989).
4. Ashton, P. R. *et al. Angew. Chem. int. Edn engl.* **30,** 1039–1042 (1991).
5. Ashton, P. R. *et al. Angew. Chem. int. Edn engl.* **30,** 1042–1044 (1991).
6. Anelli, P. L. *et al. J. Am. chem. Soc.* **114,** 193–218 (1992).
7. Hunter, C. A. *J. Am. chem. Soc.* **114,** 5303–5311 (1992).
8. Vögtle, F., Meier, S. & Hoss, R. *Angew. Chem. int. Edn engl.* **31,** 1619–1622 (1992).
9. Ogino, H. *J. Am. chem. Soc.* **103,** 1303–1304 (1981).
10. Harada, A., Li, J. & Kamachi, M. *Nature* **356,** 325–327 (1992).
11. Anelli, P. L., Spencer, N. & Stoddart, J. F. *J. Am. chem. Soc.* **113,** 5131–5133 (1991).
12. *Molecular Electronic Devices* (eds Carter, F. L. & Siatowski, R. E.) (North-Holland, Amsterdam, 1988).
13. Fujita, M., Nagao, S., Iida, M., Ogata, K. & Ogura, K. *J. Am. chem. Soc.* **115,** 1574–1576 (1993).
14. Fujita, M., Yazaki, J. & Ogura, K. *Chem. Lett.* 1031–1032 (1991).
15. *Fujita, M., Yazaki, J. & Ogura, K. J. Am. chem. Soc.* **112,** 5645–5647 (1990).

ACKNOWLEDGEMENTS. We thank M. Kanai for ESMS measurement, and T. Kuramochi and H. Seki for FABMS and NMR measurements, respectively. Support by Japan Tobacco Inc. is gratefully acknowledged. This work was supported by the Ministry of Education, Science and Culture, Japan.

An oscillation in the global climate system of period 65–70 years

Michael E. Schlesinger & Navin Ramankutty

Department of Atmospheric Sciences,
University of Illinois at Urbana-Champaign,
105 South Gregory Avenue, Urbana, Illinois 61801, USA

In addition to the well-known warming of ~0.5 °C since the middle of the nineteenth century, global-mean surface temperature records[1–4] display substantial variability on timescales of a century or less. Accurate prediction of future temperature change requires an understanding of the causes of this variability; possibilities include external factors, such as increasing greenhouse-gas concentrations[5–7] and anthropogenic sulphate aerosols[8–10], and internal factors, both predictable (such as El Niño[11]) and unpredictable (noise[12,13]). Here we apply singular spectrum analysis[14 20] to four global-mean temperature records[1–4], and identify a temperature oscillation with a period of 65–70 years. Singular spectrum analysis of the surface temperature records for 11 geographical regions shows that the 65–70-year oscillation is the statistical result of 50–88-year oscillations for the North Atlantic Ocean and its bounding Northern Hemisphere continents. These oscillations have obscured the greenhouse warming signal in the North Atlantic and North America. Comparison with previous observations and model simulations suggests that the oscillation arises from predictable internal variability of the ocean–atmosphere system.

For prescribed greenhouse-gas (GHG) and anthropogenic-sulphate-aerosol (ASA) radiative forcing, the global-mean temperature changes simulated by our simple hemispherically resolved climate/ocean model[9,10] for a range of climate sensitivities, $\Delta T_{2\times}$, are compared to the IPCC-observed global-mean surface temperature changes over 1858–1992 (ref. 1); the $\Delta T_{2\times}$ which minimizes the r.m.s. error is determined. The ASA radiative forcing, characterized by its value in 1978, $\Delta F_{SO4}(1978)$, is chosen to minimize the r.m.s. error between the simulated and observed interhemispheric temperature differences. The simulated global-mean temperature changes are then subtracted from the observed global-mean temperature changes to reveal what is not caused by GHG and ASA radiative forcing. The resulting detrended temperature changes (Fig. 1*d*) indicate the presence of a non-random, oscillatory component.

We use singular spectrum analysis (SSA)[14 20] to investigate this oscillatory component. (See Fig. 1 caption for an explanation of the quantities used in the following discussion.) Figure 1*a* shows the normalized eigenvalues λ_k, together with the 95% confidence interval, $\delta\lambda_k = 2\lambda_k(2/N)^{1/2}$(refs 15,16), where N is the length of the observational record (data set) in years. Modes 1 and 2 form a pair which contribute 28.7% of the total variance. Vautard and Ghil[16] and Vautard *et al.*[17] have argued that such an eigenvalue pair is indicative of an oscillation. The distance of modes 1 and 2 above the 'noise floor' also indicates that these modes are deterministic rather than stochastic[16,17]. Figure 1*b* presents eigenvectors ρ_1 and ρ_2, each of which exhibits a quasi-periodic structure. Figure 1*c* shows the time series for modes 1 and 2, $\hat{X}_1(t_j)$ and $\hat{X}_2(t_j)$, $j = 2, \ldots, N$. Figure 1*d* presents $\hat{X}_1(t_j) + \hat{X}_2(t_j)$ in comparison with the detrended temperature anomaly. It is seen that $\hat{X}_1(t_j) + \hat{X}_2(t_j)$ has an oscillatory structure, with a timescale $\tau \approx 65$ yr.

The oscillation revealed in Fig. 1 has not been reported in the previous SSA studies[18–20] of the global surface temperature anomaly data of Jones *et al.*[2]. This is because those analyses were performed on the non-detrended data. To demonstrate this, we applied SSA to the non-detrended data of Jones *et al.*; we also analysed the non-detrended IPCC data and obtained very similar results. Reference 18 attributed modes 1 and 2 to the trend. Our singular spectrum analysis shows instead that mode 1 primarily represents the trend and secondarily the oscillation, and *vice versa* for mode 2. When SSA is applied to such a non-detrended time series, the first mode must explain the dominating variance contributed by the trend (62%), thereby masking within it the smaller variance contributed by the oscillation (8.4%). In detrending the temperature anomaly data, we removed the need for mode 1 to explain the variance of the trend, thereby leaving it free, together with mode 2, to explain the oscillation. We have confirmed these results by applying SSA to a time series composed of a linear trend and a sine wave. Consequently, we conclude that in using SSA, any deterministic trend should first be removed from the time series.

We have also applied SSA to the observed temperature anomaly data sets of Jones *et al.*[2], Hansen and Lebedeff[3], and Vinnikov[4], each revised and updated through 1992. The $\hat{X}_1(t_j) + \hat{X}_2(t_j)$ for each data set displays an oscillatory character, with good agreement between the values for the data of Hansen and Lebedeff, and Vinnikov, and separately between IPCC and Jones *et al.*. The differences between $\hat{X}_1(t_j) + \hat{X}_2(t_j)$ for the two pairs of data sets reflect the differences between the temperature observations themselves. The first pair of data sets (Hansen and Lebedeff, and Vinnikov) consist of land surface-air temperatures alone and begin in 1880 and 1881, whereas the second pair (IPCC and Jones *et al.*) also include sea surface temperatures (SST) and begin in 1858 and 1854. Estimation of τ from these four data sets over 1881–1992 yields 65, 66, 70 and 69 yr, respectively. Because the four time series are not longer than 2τ, however, these estimates must be considered as provisional and subject to revision when longer records become available.

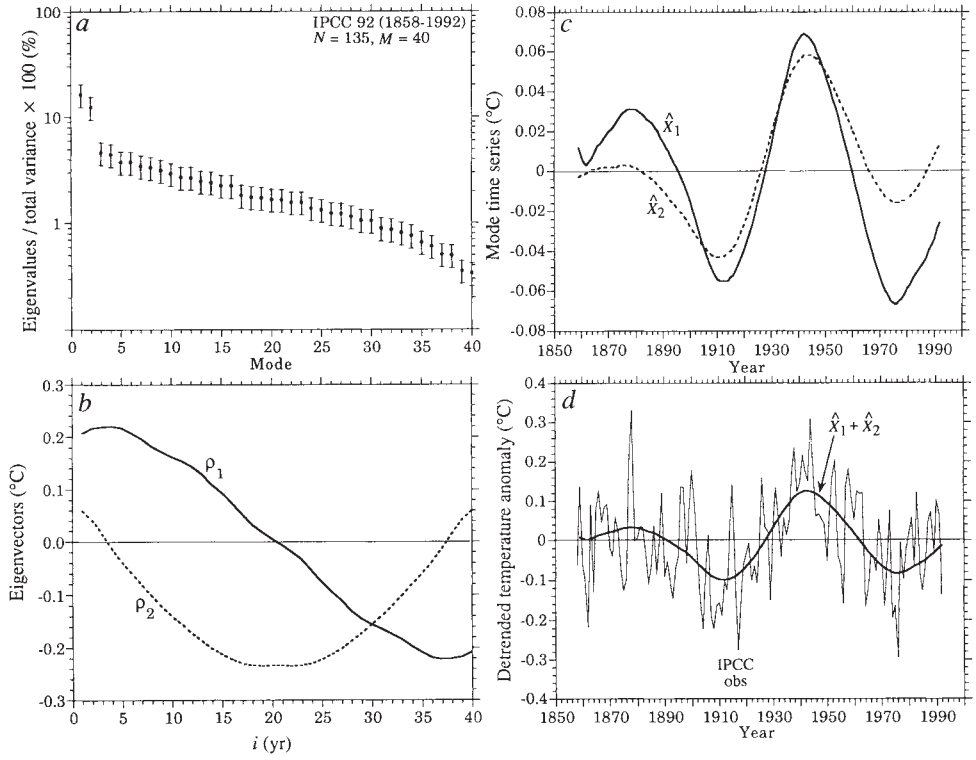

FIG. 1 *a–d*, Singular spectrum analysis (SSA) results for the IPCC global-mean temperature anomaly data[1], detrended for the global-mean response simulated by our simple climate/ocean model for GHG and ASA ($\Delta F_{SO4}(1978) = -0.35$ W m^{-2}) forcing, with $\Delta T_{2\times} = 2.21$ °C. See text for discussion of these results. Symbols used here are defined below.

METHODS. The eigenvalues λ_k and eigenvectors ρ_k, $k = 1, \ldots, M$, of the scaled autocovariance matrix, C, a Toeplitz matrix with first row,

$$C_{1,l+1} = \frac{1}{M}\frac{1}{N-l}\sum_{j=1}^{N-l} X_j X_{j+l},$$

$l = 0, \ldots, M-1$, have been determined, where $X_j = X(t_j) - \bar{X}; t_j = t_0 + j; j = 1, \ldots, N; \bar{X}$ is the average of the detrended temperature anomaly, $X(t_j)$; and $M-1$ is the maximum number of lags l. The eigenvalues λ_k, divided by the variance of X_j, give the contribution of each eigenvector ρ_k to the variance. The eigenvectors $\rho_{k,i}$, $i = 1, \ldots, M$, or empirical orthogonal functions (EOFs)[16–18], represent the temporal structure of each mode k. The time series for mode k is given by

$$\hat{X}_k(t_j) = \frac{1}{j-1}\sum_{i=1}^{j-1} A_{k,j-i}\rho_{k,i}$$

for $j = 2, \ldots, M$;

$$\frac{1}{M}\sum_{i=1}^{M} A_{k,j-i}\rho_{k,i}$$

for $j = M+1, \ldots, N-M+1$, and

$$\frac{1}{M-j+1}\sum_{i=1}^{M} A_{k,j-1}\rho_{k,i}$$

for $j = N-M+2, \ldots, N$, where

$$A_{k,j} = \sum_{i=1}^{M} X_{j+i}\rho_{k,i}$$

is the amplitude, or principal component (PC)[16–18], of mode k at time t_j. For the IPCC data, $t_0 = 1857$, $N = 135$ and $\bar{X} = -4.67 \times 10^{-8}$ °C. Following refs 18–20, we choose $M = 40$; similar results are obtained for $30 \leqslant M \leqslant 50$.

To examine whether the oscillation exists globally or only in particular geographical regions, we subdivide the Earth's surface into 11 regions as shown in Fig. 2. For each region, a history of GHG + ASA-induced temperature change is obtained by area-weighting the surface-temperature changes simulated by our simple model for ocean and land in each hemisphere. This history is then subtracted from the Jones *et al.*[2] 5° × 5° latitude–longitude gridded observed temperature anomaly data[21], averaged for each region, and the resulting detrended record is analysed by SSA.

Figure 2 reveals an oscillation in the North Atlantic region with $\tau \approx 76$ yr, an explained variance for the detrended North Atlantic temperature record of 54.8%, and a correlation coefficient with mode 1 plus mode 2 of the detrended global-mean temperature record of 0.95. Long-timescale oscillations are also found for the Northern Hemisphere continental regions bounding the North Atlantic Ocean—North America, Eurasia and Africa—with $\tau \approx 88$, 84 and 50 yr, respectively. The regional eigenvalues, eigenvectors and principal components for modes higher than two (not presented) show that oscillations with timescales as long as these do not exist elsewhere. In the Southern Hemisphere regions there are shorter-timescale oscillations, with $9 \leqslant \tau \leqslant 20$ yr, the latter for the eastern equatorial Pacific and South Pacific regions. The regional eigenvalues, eigenvectors and principal components for modes higher than two show that such short-timescale oscillations also exist in Eurasia and Africa. Thus the 20-yr oscillation in global-mean temperature, whose existence has been argued in refs 18–20, does not exist everywhere.

Figure 2 suggests some residual trend for the South Atlantic region. This is a consequence of using the hemispheric-mean temperature changes simulated by our simple model, separately for land and ocean, to detrend the observed regional temperature anomalies. Eventually, improvements in detrending might be achieved by using the geographical distribution of temperature change simulated by a calibrated atmosphere–ocean general circulation model for the time-dependent GHG and ASA forcing since 1850. It is preferable at present to apply SSA to an imperfectly detrended time series than to the non-detrended time series. The details of the regional oscillations shown in Fig. 2 should, however, be treated with caution.

The geographical structure of the oscillation is revealed in Fig. 3 by the product of the differences of 20-yr-averaged temperature anomalies, centred at the extrema of global-mean oscillation. The oscillation is seen to exist over the North Atlantic Ocean, North America, western Eurasia and northern Africa, and not to exist over most of the Southern Hemisphere where data exist back to 1900.

Figures 2 and 3 show that the 65–70-yr oscillation in global-mean temperature is the statistical result of the regional long-timescale oscillations which occur exclusively in the Northern Hemisphere. The 65–70-yr timescale of the irregular 'global' oscillation lies within the timescale band of these regional oscillations, 50–88-yr; the peak-to-peak range of the 'global' oscillation, 0.19 °C, is reduced by 75% compared to the maximum regional peak-to-peak range, 0.75 °C, for the North Atlantic region.

There are three possible sources for the 65–70-yr 'global' oscillation: (1) random forcing, such as by white noise; (2) external oscillatory forcing, such as by a variation in the solar constant; and (3) an internal oscillation of the atmosphere–ocean system. Atmospheric white-noise forcing of the ocean, evoking a red-noise response, was proposed by Hasselmann[22] and has been invoked to explain the non-GHG + ASA component of the observed temperature record[12]. Putative variations in the solar constant have also been proposed to explain this[23,24,10]. But it is unlikely that either of these forcings is the source of the 65–70-

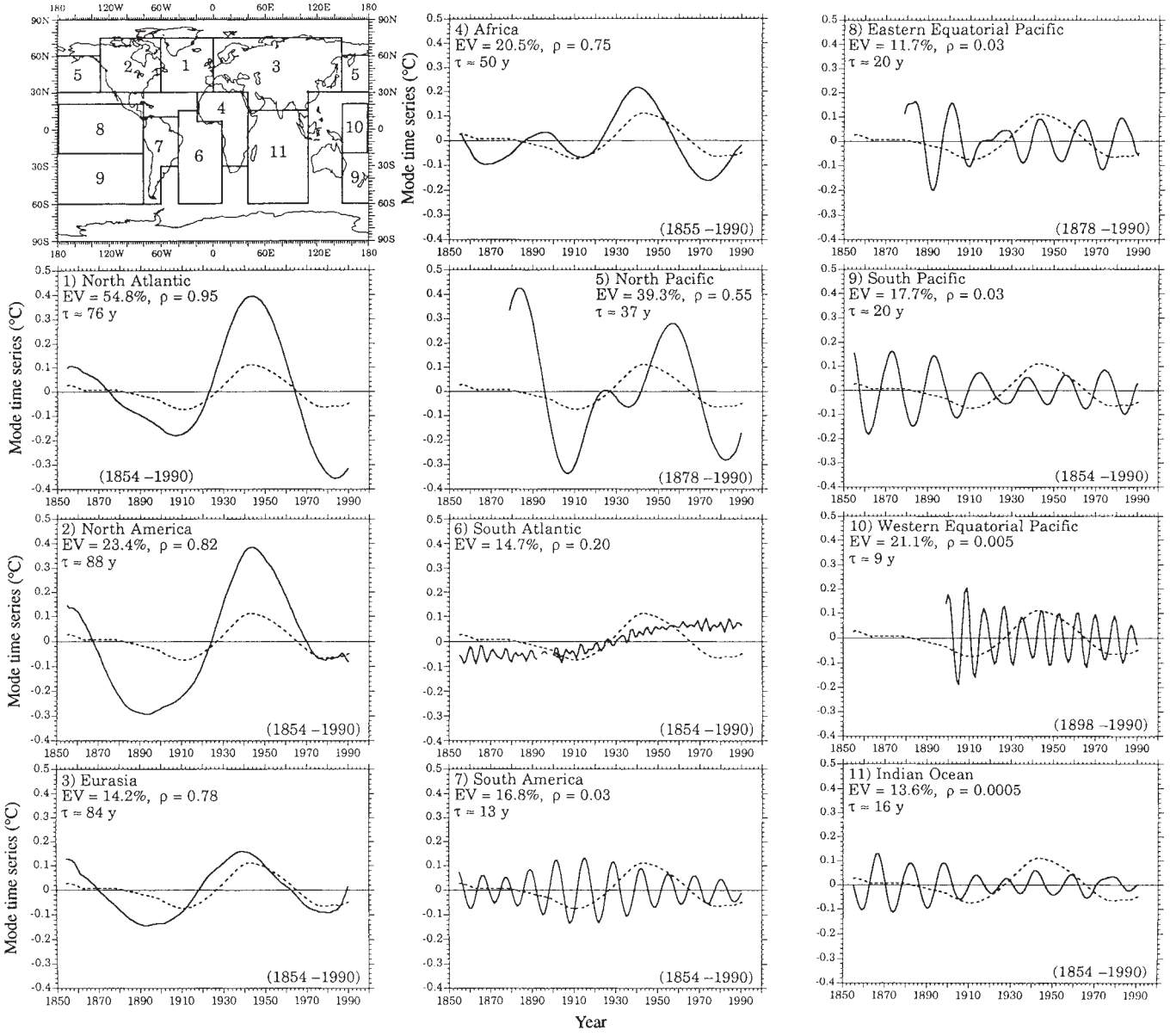

FIG. 2 SSA results for the Jones *et al.*[2] gridded temperature anomaly data[24] ($M = 40$) for the 11 regions shown (top left), each detrended for its area-weighted land and ocean hemispheric response simulated by our simple climate/ocean model for GHG and ASA ($\Delta F_{SO4}(1978) = -0.37$ W m^{-2}) forcing, with $\Delta T_{2\times} = 2.58$ °C. (Each panel (1–11) corresponds to one of the 11 regions). The contribution to the detrended temperature record by the two SSA modes which explain the largest amount of its variance, $\tilde{X}_1 + \tilde{X}_2$, is shown for each region (solid line) and for the Jones *et al.*[2] global-mean temperature anomaly (dashed line). Symbols used are as follows: the regional variance explained by the regional $\tilde{X}_1 + \tilde{X}_2$ is EV. The correlation coefficient between the regional and global-mean $\tilde{X}_1 + \tilde{X}_2$s is ρ. The timescale for the regional $\tilde{X}_1 + \tilde{X}_2$, τ, was estimated by the average time between consecutive maxima and between consecutive minima.

yr oscillation—solar forcing should generate a global response[25,26] and white-noise forcing an ocean-wide response, but the 65–70-yr oscillation is neither global nor pan-oceanic. The most probable cause of this oscillation is therefore an internal oscillation of the atmospheric–ocean system.

This conclusion is supported by a growing body of observational evidence and model-simulation results. Bjerknes (1964)[27] analysed North Atlantic SST data spanning 1894–1934 and found basin-wide interdecadal differences. Levitus (1989)[28] analysed North Atlantic hydrographic temperature and salinity data spanning 1955–74 and found coherent interdecadal differences from the sea surface down to at least 2,000 m depth. Kushnir (1994)[29] analysed a century of SST data from the Comprehensive Ocean–Atmosphere Data Set for the North Atlantic and found a long-term fluctuation, with negative anomalies before 1920, positive anomalies between 1930 and 1960, and cold anomalies in the 1970s and 80s. Delworth *et al.* (1994)[30] performed a 600-yr-long simulation with a global atmosphere–ocean general circulation model and obtained an irregular oscillation of SST and the thermohaline circulation in the North Atlantic having a timescale of ~40–60 yr.

Comparison of the regional and global-mean temperature changes induced by GHG + ASA forcing with those caused by the oscillation shows the rapid rise in global-mean temperature between about 1908 and 1946, and the subsequent reversal of this warming until about 1965, were the result of the oscillation in regions 1–4 of Fig. 2. In the North Atlantic and North American regions the oscillation has so far dominated the GHG + ASA-induced warming, thereby obscuring the latter and confounding its detection[31]. It is likely that this North Atlantic

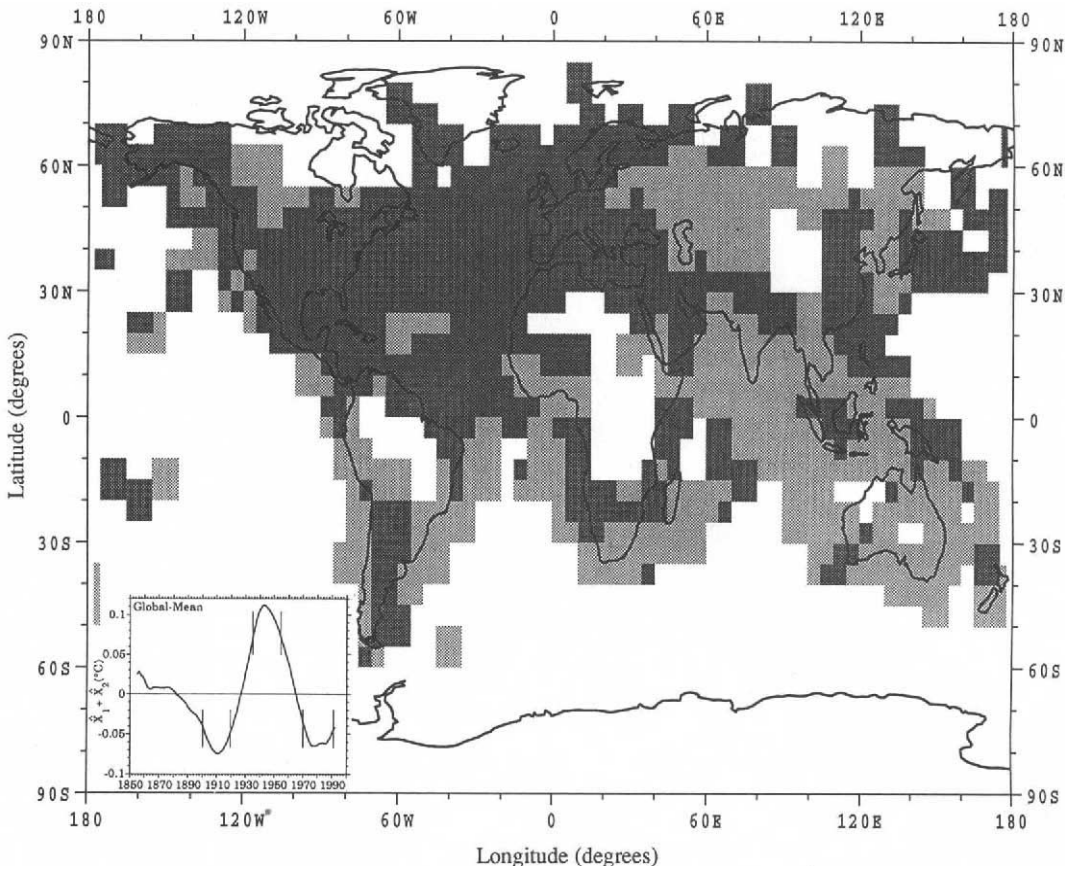

FIG. 3 Geographical distribution of the product of the differences of 20-yr-averaged temperature anomalies, centred at the extrema of global-mean oscillation (inset): [(1900–20) − (1935–55)] × [(1935–55) − (1970–90)]. The negative (positive) product, shown by dark (light) shading, is where the temperature anomaly changed (did not change) from negative during 1900–20 to positive during 1935–55 and back to negative during 1970–90. in non-shaded regions there is no product because data are absent during at least one of the 20-yr averaging periods.

oscillation has also influenced past climates as revealed by the recent Greenland ice-core analyses[32–34]. It is to be hoped that the future course of this oscillation can be predicted by atmosphere–ocean general circulation models. □

Received 29 September; accepted 30 December 1993.

1. Folland, C. K., *et al.* in *Climate Change 1992—The Supplementary Report to the IPCC Scientific Assessment* (eds Houghton, J. T., Callander, B. A. & Varney, S. K.) 135–170 (Cambridge Univ. Press, 1992).
2. Jones, P. D., Wigley, T. M. L. & Farmer, G. in *Greenhouse-Gas-Induced Climatic Change: A Critical Appraisal of Simulations and Observations.* (ed. Schlesinger, M. E.) 153–172 (Elsevier, Amsterdam, 1991).
3. Hansen, J. & Lebedeff, S. *Geophys. Res. Lett.* **15,** 323–326 (1988).
4. Vinnikov, K. Ya., Groisman, P. Ya. & Lugina, K. M. *J. Clim.* **3,** 662–677 (1990).
5. Houghton, J. T., Jenkins, G. J. & Ephraums, J. J. (eds) *Climate Change: The IPCC Scientific Assessment* (Cambridge Univ. Press, 1990).
6. Houghton, J. T., Callander, B. A. & Varney, S. K. (eds) *Climate Change 1992—The Supplementary Report to the IPCC Scientific Assessment* (Cambridge Univ. Press, 1992).
7. Wigley, T. M. L. & Raper, S. C. B. *Nature* **357,** 293–300 (1992).
8. Wigley, T. M. L. *Nature* **339,** 365–367 (1989).
9. Schlesinger, M. E., Jiang, X. & Charlson, R. J. in *Climate Change and Energy Policy: Proceedings of the International Conference on Global Climate Change: Its Mitigation Through Improved Production and Use of Energy* (eds Rosen, L. & Glasser, R.) 75–108 (Am. Inst. Phys., New York, 1992).
10. Schlesinger, M. E. & Ramankutty, N. *Nature* **360,** 330–333 (1992).
11. Quinn, W. H. & Neal, V. T. *J. geophys. Res.* **92,** 14449–14461 (1987).
12. Wigley, T. M. L. & Raper, S. C. B. *Nature* **344,** 324–327 (1990).
13. Bloomfield, P & Nychka, D. *Clim. Change* **21,** 275–287 (1992).
14. Broomhead, D. S. & King, G. P. *Physica* **20D,** 217–236 (1986).
15. Fraedrich, K. *J. atmos. Sci.* **43,** 419–432 (1986).
16. Vautard, R. & Ghil, M. *Physica* **35D,** 395–424 (1989).
17. Vautard, R., Yiou, P. & Ghil, M. *Physica* **58D,** 95–126 (1992).
18. Ghil, M. & Vautard, R. *Nature* **350,** 324–327 (1991).
19. Elsner, J. B. & Tsonis, A. A. *Nature* **353,** 551–553 (1991).
20. Allen, M. R., Read, P. L. & Smith, L. A. *Nature* **355,** 686 (1992).
21. *Greenhouse Effect Detection Experiment* CD-ROM (NASA Goddard Space Flight Center, Greenbelt, Maryland 1992).
22. Hasselmann, K. *Tellus,* 473–485 (1976).
23. Friis-Christensen, E. & Lassen, K. *Science* **254,** 698–700 (1991).
24. Kelly, P. M. & Wigley, T. M. L. *Nature* **360,** 328–330 (1992).
25. Wetherald, R. T. & Manabe, S. *J. atmos. Sci.* **32,** 2044–2059 (1975).
26. Nesme-Ribes, E., Ferreira, E. N., Sadourny, R., Le Treut, H. & Li, Z. X. *J. geophys. Res.* **98,** 18923–18935 (1993).
27. Bjerknes, J. in *Advances in Geophysics* Vol. 10 (eds Landsberg, H. E. & Van Mieghem, J.) 1–82 (Academic, New York, 1964).
28. Levitus, S. *J. geophys. Res.* **94,** 6091–6131 (1989).
29. Kushnir, Y. *J. Clim.* **7,** 141–157 (1994).
30. Delworth, T., Manabe, S. & Stouffer, R. J. *J. Clim.* **6,** 1993–2011 (1993).
31. Michaels, P. J. *Bull. Am. met. Soc.* **73,** 1563–1577 (1992).
32. Taylor, K. C. *et al. Nature* **361,** 432–436 (1993).
33. Greenland Ice-core Project (GRIP) Members *Nature* **364,** 203–207 (1993).
34. Dansgaard, W. *et al. Nature* **364,** 218–220 (1993).

ACKNOWLEDGEMENTS. We thank D. Parker for providing the IPCC data, P. Jones and M Hulme for providing the Jones *et al.* data, J. Hansen and H. Wilson for providing the Hansen and Lebedeff data, K. Vinnikov for providing his data, and M. Althouse for comments. This work was supported by the US NSF and the US Department of Energy.

Relationship of baleen whales established by cytochrome *b* gene sequence comparison

Úlfur Árnason & Anette Gullberg

Department of Genetics,
Division of Evolutionary Molecular Systematics, University of Lund,
Sölvegatan 29, S-223 62 Lund, Sweden

A RECENT revision[1] of whale phylogeny suggested that the sperm whale was more closely related to rorquals than to other toothed whales. This made the suborder Odontoceti (toothed whales) paraphyletic, and implied that the latest common ancestor of rorquals and sperm whales may have lived only 10–13 million years ago. This is at variance with palaeontological evidence for the greater antiquity for both mysticetes (baleen whales) and sperm whales, so the Mysticeti, as well as the Odontoceti, must also be paraphyletic if the dates implied in ref. 1 were correct. Here we present a more comprehensive phylogenetic analysis that demonstrates the monophyly of mysticetes and identifies no particular affinity between the sperm whales and rorquals.

The Odontoceti and the Mysticeti are generally considered to